J. Fluid Mech. (1987), *vol.* 176, *pp.* 221–235
Printed in Great Britain

The evolution of instabilities in the axisymmetric jet. Part 2. The flow resulting from the interaction between two waves

By J. COHEN† AND I. WYGNANSKI‡
Aerospace and Mechanical Engineering Department, University of Arizona, Tucson, AZ 85721, USA

(Received 11 February 1986)

Leading nonlinear interactions generated by waves externally superimposed on an axisymmetric jet are considered theoretically, and the results verified experimentally. The mean flow in the jet loses its axial symmetry whenever the jet is excited simultaneously by two different azimuthal modes of the same frequency. Subharmonic resonance occurs in this flow whenever the conditions warrant such an occurrence, generating azimuthal modes which may not have been present otherwise in this flow. Some of these resonance conditions are explored.

1. Introduction

The linear aspects of the inviscid instabilities governing the amplification of wavy disturbances in an axisymmetric jet have discussed in the first part of this paper (Cohen & Wygnanski 1987). The model proposed predicts quite well the frequency of the most energetic waves, their azimuthal modes, the lateral distribution of their amplitudes and phases, and the development of the spectral distribution of the fluctuating velocities over short distances in the direction of streaming.

The linear stability theory predicts that a continuous spectrum of waves corresponding to a broad band of frequencies (Michalke 1965) and a large number of discrete azimuthal modes (Plaschko, 1979; Cohen & Wygnanski 1987) are exponentially amplified with increasing distance from the nozzle. The unstable modes therefore attain amplitudes that are sufficiently high for the nonlinear terms arising in the equations of motion to become significant. The inclusion of the leading nonlinearities in the stability analysis alters the mean flow, which in turn affects the linear evolution of the disturbances; it may also be responsible for the creation of second-order interactions between two types of waves which may resonate at times (Kelly 1967), resulting in a rapid transfer of energy from one wave to another. The most common nonlinear interaction between two waves involves the fundamental wave and its various harmonic and subharmonic components, but a resonant interaction between waves having differing azimuthal modes may also occur and may be responsible for the generation of new modes that were not initially present.

The modification to the mean flow resulting from the interaction between two azimuthal modes is analysed in detail and so are the resonance conditions responsible for the generation of new modes. The mathematical analysis is supplemented by

† Present address: Department of Aeronautics & Astronautics, Massachusetts Institute of Technology, Cambridge, MA 02139, USA.
‡ Also: School of Engineering, Tel Aviv University, Tel Aviv, Israel.

experiments carried out in a flow of air emanating from a circular nozzle. The experimental apparatus, the techniques of data acquisition, and the flow conditions are described by Cohen & Wygnanski (1987).

2. Analysis

2.1. *Mathematical formulation of the leading nonlinearities*

Let U be the velocity vector representing the flow in an axisymmetric jet having components U, V and W in cylindrical coordinates $\boldsymbol{x}(x, r, \phi)$. The momentum and continuity equations for incompressible, inviscid flow are

$$\frac{\partial U}{\partial t}+V\frac{\partial U}{\partial r}+\frac{W}{r}\frac{\partial U}{\partial \phi}+U\frac{\partial U}{\partial x}=-\frac{1}{\rho}\frac{\partial P}{\partial x}, \tag{2.1a}$$

$$\frac{\partial V}{\partial t}+V\frac{\partial V}{\partial r}+\frac{W}{r}\frac{\partial V}{\partial \phi}-\frac{W^2}{r}+U\frac{\partial V}{\partial x}=-\frac{1}{\rho}\frac{\partial P}{\partial r}, \tag{2.1b}$$

$$\frac{\partial W}{\partial t}+V\frac{\partial W}{\partial r}+\frac{W}{r}\frac{\partial W}{\partial \phi}+\frac{WV}{r}+U\frac{\partial W}{\partial x}=-\frac{1}{\rho r}\frac{\partial P}{\partial \phi}, \tag{2.1c}$$

$$r\frac{\partial V}{\partial r}+V+\frac{\partial W}{\partial \phi}+r\frac{\partial U}{\partial x}=0, \tag{2.1d}$$

where P represents the pressure field and ρ is the fluid density. Assuming that the mean flow, which is neither divergent nor swirling [i.e. it has velocity components $\overline{U}=(\overline{U}_0(r), 0, 0)$], is subjected to two small disturbances simultaneously, one may express the flow-field vector $\boldsymbol{q}$ by the following expansion:

$$\boldsymbol{q}(x, r, \phi, t)=\boldsymbol{q}_0(r)+\epsilon_{11}\boldsymbol{q}_{11}(x, r, \phi, t)+\epsilon_{12}\boldsymbol{q}_{12}(x, r, \phi, t)+\epsilon^2\boldsymbol{q}_2(x, r, \phi, t)+O(\epsilon^3), \tag{2.2}$$

which can be rewritten in scalar form as follows:

$$\begin{bmatrix} U(x, r, \phi, t) \\ V(x, r, \phi, t) \\ W(x, r, \phi, t) \\ (1/\rho)P(x, r, \phi, t) \end{bmatrix}=\begin{bmatrix} \overline{U}_0(r) \\ 0 \\ 0 \\ 0 \end{bmatrix}+\epsilon_{11}\begin{bmatrix} u_{11}(x, r, \phi, t) \\ v_{11}(x, r, \phi, t) \\ w_{11}(x, r, \phi, t) \\ p_{11}(x, r, \phi, t) \end{bmatrix}$$

$$+\epsilon_{12}\begin{bmatrix} u_{12}(x, r, \phi, t) \\ v_{12}(x, r, \phi, t) \\ w_{12}(x, r, \phi, t) \\ p_{12}(x, r, \phi, t) \end{bmatrix}+\epsilon^2\begin{bmatrix} u_2(x, r, \phi, t) \\ v_2(x, r, \phi, t) \\ w_2(x, r, \phi, t) \\ p_2(x, r, \phi, t) \end{bmatrix}+O(\epsilon^3), \tag{2.3}$$

where ϵ_{11} and ϵ_{12} represent the amplitudes of the two small disturbances superimposed on the mean parallel flow $[\overline{U}_0(r)]$. It is assumed that

$$0<O(\epsilon_{11})\approx O(\epsilon_{12})=O(\epsilon)\ll 1. \tag{2.4}$$

One may use the normal-mode decomposition to represent the vector $\boldsymbol{q}_{11}$ as follows:

$$\begin{aligned}\boldsymbol{q}_{11}(x, r, \phi, t)=&\,\boldsymbol{Q}_{11}^{+}(r)\exp[\mathrm{i}(\alpha_{11}x-\beta_{11}t+m_{11}\phi)]\\&+\boldsymbol{Q}_{11}^{+*}(r)\exp[-\mathrm{i}(\alpha_{11}^{*}x-\beta_{11}t+m_{11}\phi)]\\&+\boldsymbol{Q}_{11}^{-}(r)\exp[\mathrm{i}(\alpha_{11}x-\beta_{11}t-m_{11}\phi)]\\&+\boldsymbol{Q}_{11}^{-*}(r)\exp[-\mathrm{i}(\alpha_{11}^{*}x-\beta_{11}t-m_{11}\phi)],\end{aligned}$$

$$\text{or}\quad \boldsymbol{q}_{11}(x, r, \phi, t)=\boldsymbol{q}_{11}^{+}(x, r, \phi, t)+\boldsymbol{q}_{11}^{+*}(x, r, \phi, t)+\boldsymbol{q}_{11}^{-}(x, r, \phi, t)+\boldsymbol{q}_{11}^{-*}(x, r, \phi, t) \tag{2.5}$$

where β_{11} is the frequency of wave 11, m_{11} is the azimuthal mode number, and α_{11} is a complex constant whose real part (α_{11r}) gives the wavenumber and whose imaginary part (α_{11i}) determines the growth rate of wave 11. The radial distribution of the amplitude vector $\boldsymbol{Q}_{11}(r)$ is given by $\boldsymbol{Q}_{11} = [U_{11}(r), V_{11}(r), W_{11}(r), P_{11}(r)]$. The asterisk represents the complex-conjugate term; the superscripted plus and minus signs represent waves running in the positive and negative directions of the azimuthal angle. Expressing the exponential part of the disturbance by E,

$$E^{(\pm)} = \exp[\mathrm{i}(\alpha x - \beta t \pm m\phi)], \tag{2.6}$$

the vector $\boldsymbol{q}_{11}$, and similarly $\boldsymbol{q}_{12}$ and $\boldsymbol{q}_2$, may be written as

$$\boldsymbol{q}_{11}(x, r, \phi, t) = \boldsymbol{Q}_{11}^{+}(r)\, E_{11}^{+} + \boldsymbol{Q}_{11}^{-}(r)\, E_{11}^{-} + (*), \tag{2.7a}$$

$$\boldsymbol{q}_{12}(x, r, \phi, t) = \boldsymbol{Q}_{12}^{+}(r)\, E_{12}^{+} + \boldsymbol{Q}_{12}^{-}(r)\, E_{12}^{-} + (*), \tag{2.7b}$$

$$\boldsymbol{q}_{2}(x, r, \phi, t) = \boldsymbol{Q}_{2}^{+}(r)\, E_{2}^{+} + \boldsymbol{Q}_{2}^{-}(r)\, E_{2}^{-} + (*). \tag{2.7c}$$

When (2.3) is substituted into (2.1) and the linear superposition property is used to order ϵ, the following equation is obtained:

$$\mathrm{L_p}(\boldsymbol{q}_{11}^{+}) = \begin{bmatrix} \dfrac{\partial}{\partial t} + \overline{U}_0 \dfrac{\partial}{\partial x} & \overline{U}_0' & 0 & \dfrac{\partial}{\partial x} \\ 0 & \dfrac{\partial}{\partial t} + \overline{U}_0 \dfrac{\partial}{\partial x} & 0 & \dfrac{\partial}{\partial r} \\ 0 & 0 & \dfrac{\partial}{\partial t} + \overline{U}_0 \dfrac{\partial}{\partial x} & \dfrac{1}{r}\dfrac{\partial}{\partial \phi} \\ r\dfrac{\partial}{\partial x} & 1 + r\dfrac{\partial}{\partial r} & \dfrac{\partial}{\partial \phi} & 0 \end{bmatrix} \begin{pmatrix} u_{11}^{+} \\ v_{11}^{+} \\ w_{11}^{+} \\ p_{11}^{+} \end{pmatrix} = \mathbf{0}, \tag{2.8}$$

where $\mathrm{L_p}$ is a linear partial differential operator applied to $\boldsymbol{q}_{11}^{+}$, and the ordinary derivative with respect to r is denoted by a prime. The equations for $\boldsymbol{q}_{11}^{-}$, $\boldsymbol{q}_{12}^{+}$, $\boldsymbol{q}_{12}^{-}$, and $\boldsymbol{q}_2^{+}$ and their complex-conjugate vectors are the same. Substitution of (2.5) into (2.8) yields

$$\mathrm{L_0}(\boldsymbol{Q}_{11}^{+}) = \begin{bmatrix} \overline{U}_0 - c_{11} & -\dfrac{\mathrm{i}}{\alpha_{11}}\overline{U}_0' & 0 & 1 \\ 0 & \overline{U}_0 - c_{11} & 0 & -\dfrac{\mathrm{i}}{\alpha_{11}}\dfrac{d}{dr} \\ 0 & 0 & \overline{U}_0 - c_{11} & \dfrac{m_{11}}{r\alpha_{11}} \\ 1 & -\dfrac{\mathrm{i}}{\alpha_{11}}\left(\dfrac{d}{dr} + \dfrac{1}{r}\right) & \dfrac{m_{11}}{r\alpha_{11}} & 0 \end{bmatrix} \begin{pmatrix} U_{11}^{+} \\ V_{11}^{+} \\ W_{11}^{+} \\ P_{11}^{+} \end{pmatrix} = \mathbf{0}, \tag{2.9}$$

where $\mathrm{L_0}(\boldsymbol{Q}_{11}^{+})$ is the linear ordinary differential operator applied to $\boldsymbol{Q}_{11}^{+}$ and c_{11} is defined by $c_{11} = \beta_{11}/\alpha_{11}$.

The equation for $\boldsymbol{Q}_{11}^{+*}$ is derived by taking the complex-conjugate of (2.9), while reversing the sign of m_{11} in (2.9) gives the equation for $\boldsymbol{Q}_{11}^{-}$.

Equation (2.9) can be reduced to a second-order ordinary differential equation for the pressure component $P_{11}^{+}(r)$, as was done by Plaschko (1979):

$$\mathrm{L}(P_{11}^{+}) \equiv P_{11}^{+\prime\prime} + \left[\frac{1}{r} - \frac{2\bar{U}_0'}{\bar{U}_0 - c_{11}}\right] P_{11}^{+\prime} - \left[\frac{m_{11}^2}{r^2} + \alpha_{11}^2\right] P_{11}^{+} = 0. \tag{2.10}$$

The equation to order ϵ^2 is given by

$$\mathrm{L}_p(\boldsymbol{q}_2) = \boldsymbol{R}, \tag{2.11}$$

where all the terms contained in vector $\boldsymbol{R}$ are the products of the linear solutions, i.e. the products of vectors $\boldsymbol{q}_{11}$ and $\boldsymbol{q}_{12}$ with themselves and the cross-product of $\boldsymbol{q}_{11}$ and $\boldsymbol{q}_{12}$ with one another. Since the homogeneous part of (2.11) is the same as (2.8), the homogeneous solution to (2.11) will add only a correction of order ϵ to the solution given by (2.5). Therefore, only the particular solution of (2.11) is considered. Moreover, since L_p is a linear operator, one checks for particular solutions corresponding to each term of the right-hand side of (2.11) separately. In the discussion that follows, the radial dependence of the particular solution is not considered and therefore *only the representative elements* of vector $\boldsymbol{R}$, showing its dependence on x, t and ϕ *are analysed. These elements* are labelled as R.H.S. in (2.12).

$$\begin{aligned}\text{R.H.S.} = {} & T_1^{\pm} \exp\{\mathrm{i}[(\alpha_{11}+\alpha_{12})x - (\beta_{11}+\beta_{12})t \pm (m_{11}+m_{12})\phi]\} \\ & + T_2^{\pm} \exp\{\mathrm{i}[(\alpha_{11}-\alpha_{12}^{*})x - (\beta_{11}-\beta_{12})t \pm (m_{11}-m_{12})\phi]\} \\ & + T_3^{\pm} \exp\{\mathrm{i}[(\alpha_{11}+\alpha_{12})x - (\beta_{11}+\beta_{12})t \pm (m_{11}-m_{12})\phi]\} \\ & + T_4^{\pm} \exp\{\mathrm{i}[(\alpha_{11}-\alpha_{12}^{*})x - (\beta_{11}-\beta_{12})t \pm (m_{11}+m_{12})\phi]\} + (*), \end{aligned} \tag{2.12a}$$

where $T_1^{\pm}$, $T_2^{\pm}$, $T_3^{\pm}$, and $T_4^{\pm}$ are functions of the radial coordinate and the eigenvalues α_{1j}, β_{1j} and m_{1j}, $j = 1, 2$, while the $\pm$ signs represent the appropriate azimuthal directions. By replacing subscript 12 with 11 in (2.12a) one obtains a term representing a second-order self-interaction of a single wave.

Whenever the disturbances are excited artificially, (2.12a) is reduced to

$$\begin{aligned}\text{R.H.S.} = {} & T_1 \exp\{\mathrm{i}[(\alpha_{11}+\alpha_{12})x - (\beta_{11}+\beta_{12})t + (m_{11}+m_{12})\phi]\} \\ & + T_2 \exp\{\mathrm{i}[(\alpha_{11}-\alpha_{12}^{*})x - (\beta_{11}-\beta_{12})t + (m_{11}-m_{12})\phi]\}. \end{aligned} \tag{2.12b}$$

2.1.1. *Mean-wave interaction*

Suppose that the jet is excited by two waves having the same frequency $\beta_{11} = \beta_{12} = \beta$. Consequently, phase-averaging of (2.11) or, equivalently, considering only the particular solution associated with the mean part (RSM) of (2.12b) yields

$$\begin{aligned}\langle\text{RHS}\rangle = \text{RSM} = {} & T_2(r; \beta, \alpha_{11}, \alpha_{12}, m_{11}, m_{12}) \\ & \times \exp[-(\alpha_{\mathrm{i},11}+\alpha_{\mathrm{i},12})x + \mathrm{i}(\alpha_{\mathrm{r},11}-\alpha_{\mathrm{r},12})x + \mathrm{i}(m_{11}-m_{12})\phi], \end{aligned} \tag{2.13}$$

where T_2 is a complex function of the radial coordinate and the eigenvalues β, α_{1j} and m_{1j}, $j = 1, 2$. We shall now consider the following cases: (i) exciting a single mode; (ii) generating standing waves; and (iii) exciting two waves having the same frequency.

(i) *Exciting a single mode.* In this case, the eigenvalues of wave 11 are the same as those of wave 12, and therefore (2.13) reduces to

$$\text{RSM} = T_2(r; \beta, \alpha, m) \exp(-2\alpha_{\mathrm{i}} x). \tag{2.14}$$

Since the right-hand side of (2.14) is independent of the azimuthal coordinate ϕ, one concludes that the azimuthal structure of the mean field of an axisymmetric jet remains axisymmetric when the jet is subjected to a single mode of excitation.

(ii) *Generating standing waves.* Standing waves are generated by exciting two waves using the following relations:

$$\beta_{11} = \beta_{12} = \beta; \quad \alpha_{11} = \alpha_{12} = \alpha; \quad m_{11} = -m_{12} = m. \tag{2.15}$$

In this case, (2.13) reduces to

$$\mathrm{RSM} = T_2(r; \beta, \alpha, m) \exp[-2\alpha_i x + 2im\phi]. \tag{2.16}$$

Substituting

$$T_2(r; \beta, \alpha, m) = |T_2(r)| \exp[\mathrm{i}\phi_0(r)], \tag{2.17}$$

where $|T_2|$ is the modulus and ϕ_0 is the phase of the complex function T_2, gives

$$\mathrm{RSM} = \exp[-2\alpha_i x]\,|T_2(r)| \exp[\mathrm{i}(2m\phi + \phi_0(r))]. \tag{2.18}$$

Since the added 'mean flow' has to be real, the real part of (2.13) is considered:

$$\mathrm{RSM}_{\mathrm{real}} = \exp[-2\alpha_i x]\,|T_2(r)| \cos(2m\phi + \phi_0(r)). \tag{2.19}$$

The particular solution associated with (2.19), and therefore with each velocity component of the added mean flow resulting from the excitation in which standing waves are generated, should vary like $\cos(2m\phi)$. This variation has a phase shift ϕ_0 depending on radial position. The amplitude of the azimuthal cosine shape grows with downstream distance and depends on the radial position as well.

(iii) *Exciting two waves having the same frequency.* In investigating this case, the limit in which the ratio between the planar momentum thickness θ and the jet radius R_j may be assumed small is considered first. Since for this limit all modes of order unity have identical solutions (Cohen & Wygnanski 1987), (2.13) can be reduced to

$$\mathrm{RSM} = T_2(r; \beta, \alpha, m_{11}, m_{12}) \exp[-2\alpha_i x + \mathrm{i}(m_{11} - m_{12})\phi]. \tag{2.20}$$

Thus, providing that the effective azimuthal mode number $2m$ appearing in (2.18) is replaced by the difference between the two azimuthal mode numbers $m_{11} - m_{12}$, in (2.20), the two cases are identical. However, the restriction to even azimuthal shapes appearing in (2.18) no longer applies; 'odd' shapes are possible when $m_{11} - m_{12}$ is an odd integer.

In general, when (2.17) is used, the real part of (2.13) can be rewritten as

$$\begin{aligned}
\mathrm{RSM}_{\mathrm{real}} &= \exp[-(\alpha_{i,11} + \alpha_{i,12})x]\,|T_2(r)| \cos[(\alpha_{r,11} - \alpha_{r,12})x + (m_{11} - m_{12})\phi + \phi_0(r)] \\
&= \exp[-(\alpha_{i,11} + \alpha_{i,12})x]\,|T_2(r)| \{\cos((m_{11} - m_{12})\phi) \\
&\quad \times [\cos(\phi_0(r)) \cos((\alpha_{r,11} - \alpha_{r,12})x) - \sin(\phi_0(r)) \\
&\quad \times \sin((\alpha_{r,11} - \alpha_{r,12})x)] - \sin((m_{11} - m_{12})\phi)\,[\cos(\phi_0(r)) \\
&\quad \times \sin((\alpha_{r,11} - \alpha_{r,12})x) + \sin(\phi_0(r)) \cos((\alpha_{r,11} - \alpha_{r,12})x)]\}.
\end{aligned} \tag{2.21}$$

The resulting azimuthal shape of the added mean flow corresponding to (2.21) has the form of $\cos(m_{11} - m_{12})\phi$. The variation of this 'cosine shape' with downstream and radial coordinates is essentially the same as in case (ii). However, because of the new x-dependence arising from the difference $\alpha_{r,11} - \alpha_{r,12}$, which serves as an x-dependent phase shift, the mean azimuthal structure at a given radial position might seem to 'rotate' in the direction of streaming.

2.1.2. *Resonance conditions*

When one of the exponentials given on the right-hand side of (2.12) has the same time and spatial dependence as the homogeneous solutions of $\mathrm{L}_0(\boldsymbol{Q}_{11}) = 0$ or

$L_0(Q_{12}) = 0$, the particular solution associated with this exponential grows linearly with downstream distance and with time. This particular solution is considered to be 'secular' since it invalidates (2.2) at streamwise distances and times proportional to ϵ^{-1}. These secular terms are responsible for the resonant nonlinear interaction between the two waves.

If q_{in} represents a wave produced by the interaction between waves q_{11} and q_{12} which grows in a secular manner, the eigenvalues associated with q_{in} must satisfy one of the following resonance conditions:

$$\alpha_{in} = \alpha_{11} + \alpha_{12}; \quad \beta_{in} = \beta_{11} + \beta_{12}; \quad m_{in} = \pm(m_{11} \pm m_{12}), \tag{2.22a}$$

$$\alpha_{in} = \alpha_{11} - \alpha_{12}^*; \quad \beta_{in} = \beta_{11} - \beta_{12}; \quad m_{in} = \pm(m_{11} \pm m_{12}), \tag{2.22b}$$

and their complex-conjugate relations.

3. Experimental demonstration of the leading nonlinear interactions

3.1. *The distortion of the mean velocity field*

Exciting the jet at a single mode and frequency does not destroy the axial symmetry of the mean motion, which remains independent of the azimuthal angle ϕ (equation 2.14). To verify this statement, the jet was excited in the axisymmetric mode ($m = 0$) using a single woofer located at the bottom of the settling chamber, and independently in modes $m = +1$ and $m = +2$ with the aid of the eight acoustic drivers located near the nozzle [see Cohen & Wygnanski 1987 for details]. The exhaust velocity of the jet U_j was 8 m/s and the frequency of the excited wave was 204 Hz, resulting in a local Strouhal number ($St_\theta = F_f \theta / U_j$, where F_f represents the frequency of the forced wave) of 0.03 at $x/D = 0.65$. This value of the local Strouhal number guarantees that the excited wave is within the last stages of amplification (according to the linear stability theory) and therefore most susceptible to nonlinear interactions. Measured mean velocity profiles $\bar{U}_T(r, \phi)$ corresponding to three different types of excitation are shown in figure 1. In each case, eight profiles, taken at eight azimuthal locations 45° apart, are plotted. Figure 1 (*a*, *b*) demonstrates that the axisymmetric structure of the jet is maintained when it is subjected to a single mode of excitation, be it axisymmetric or helical, since all eight profiles collapse onto a single curve. Whenever two modes of excitation were applied simultaneously, the axisymmetric shape of the mean velocity was destroyed, as predicted in (2.20) (figure 1*c*). (Note that all the profiles shown in figure 1 (*c*) were matched at the centre of the shear layer, i.e. at the half-velocity point.)

The cosine dependence $[\cos\phi(m_{11} - m_{12})]$ of the azimuthal variation of the added mean flow was verified by subjecting the jet to two waves of the same frequency but different mode numbers m_{11} and m_{12}. Since $\theta/R_j \approx 0.04$, the assumptions made in deriving (2.20) are applicable (i.e. $\theta/R_j \ll 1$). The circumferential variation of the added mean flow was obtained by subtracting the azimuthally averaged mean velocity from the local mean velocity at each radial location. The resulting circumferential configuration was then compared to the suitable cosine shape by using the Fourier decomposition. The triangular symbols shown in figure 2 (*a*) represent the data points obtained while the jet was excited by modes 0 and +1. Six sets of data points corresponding to six different radial positions were measured and plotted. The circumferential variation of each set, which contains eight data points corresponding to eight azimuthal stations, is compared with the predicted $\cos\phi$ shape, shown by a solid line. When the jet was excited at modes 0 and +2 simultaneously, the results

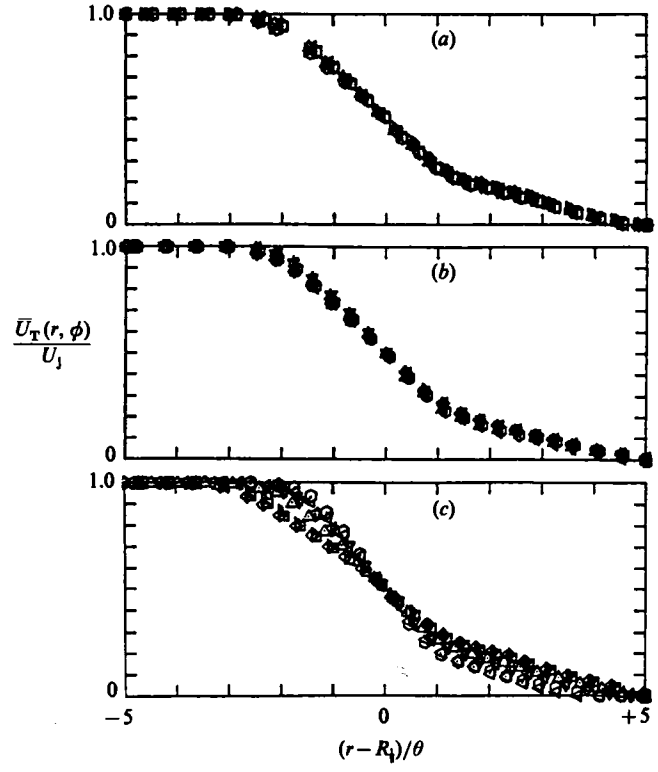

FIGURE 1. Azimuthal similarity of mean velocity profiles measured at $x/D = 0.65$, with forcing frequency of 204 Hz and mode number: (*a*) 0; (*b*) 1; (*c*) 0+1.

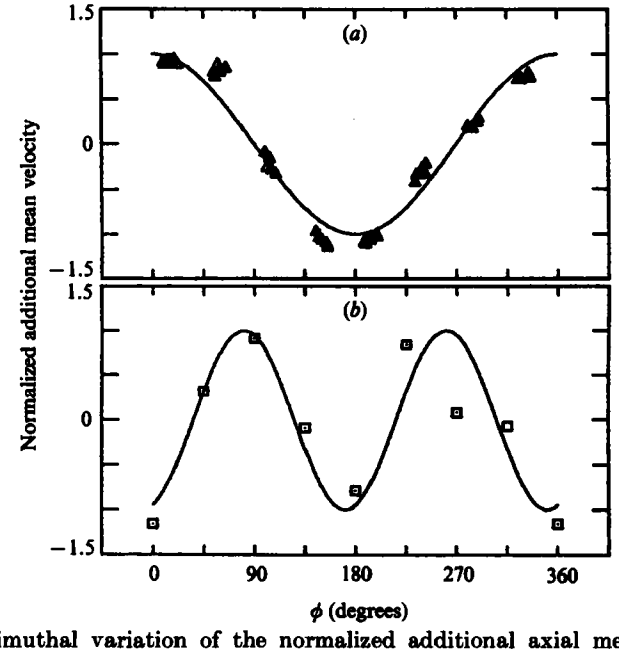

FIGURE 2. Azimuthal variation of the normalized additional axial mean velocity profiles at $x/D = 0.65$, $F_f = 204$ Hz; (*a*) △, $m = 0+1$; ——, predicted $\cos\phi$ shape; (*b*) □, $m = 0+2$; —— predicted $\cos 2\phi$ shape.

(represented by square symbols in figure 2*b*) have to be compared with the $\cos 2\phi$ shape. (Note that the first point at $\phi = 0°$ is repeated again at $\phi = 360°$.)

Contours representing the azimuthal distribution of the streamwise component of the mean velocity for various modes of excitation are plotted in figures 3 and 4. In order to calculate these contours, the following equations were solved:

$$\left.\begin{aligned} \overline{U}_{\mathrm{T}}(r,\phi) &= \overline{U}_0(r) + u_m(r,\phi); \\ \overline{U}_0(r) &= 0.5\left\{1+\tanh\left[\frac{R_{\frac{1}{2}}}{4\theta}\left(\frac{R_{\frac{1}{2}}}{r}-\frac{r}{R_{\frac{1}{2}}}\right)\right]\right\}; \\ u_m(r,\phi) &= -A(r)\cos n\phi; \end{aligned}\right\} \tag{3.1}$$

where the total mean velocity at a given distance from the nozzle $[\overline{U}_{\mathrm{T}}(r,\phi)]$ represents the superposition of the basic profile, $\overline{U}_0(r)$, and the perturbation $u_m(r,\phi)$, resulting from the interaction of helically excited waves. The basic profile used was suggested by Michalke (1971). The perturbation velocity is given by a cosine function, where n stands for the difference between the mode numbers of the excited waves. The dependence of the perturbed profile on the radial coordinate relative to the azimuthal $\cos n\phi$ variation is neglected; therefore $A(r)$, whose magnitude is related to the amplitude of the excited waves, is taken to be a constant. A straightforward algebraic procedure for a given mean velocity contour level, say U_{ac}, leads to the following equations:

$$\left.\begin{aligned} \frac{r}{R_{\frac{1}{2}}} &= 0.5\left[-\hat{y}+(\hat{y}^2+4)^{\frac{1}{2}}\right], \\ \hat{y} = \frac{R_{\frac{1}{2}}}{r}-\frac{r}{R_{\frac{1}{2}}} &= 2\frac{\theta}{R_{\frac{1}{2}}}\ln\left[\frac{1+2(U_{\mathrm{ac}}-0.5)+2A\cos n\phi}{1-2(U_{\mathrm{ac}}-0.5)-2A\cos n\phi}\right]. \end{aligned}\right\} \tag{3.2}$$

Four contour plots, calculated for $n = 1, 2, 3$ and 4, are shown in figure 3. For each value of n, two contours are plotted. The solid curve represents a relatively low level of excitation, while the dashed line corresponds to a disturbance having a higher amplitude. In each case, the solid curves resemble a canonical configuration (a circle whose centre does not coincide with the nozzle, an ellipse, a triangle and a square) and the dashed lines represent a combination of the number of n of lobes. In order to accentuate the azimuthal structure in figure 3 a circle of radius $0.9{*}R_{\min}$ was subtracted from each contour shown in this figure. $R_{\min}$ represents the minimum distance between the original contour and the centre of the jet.

A comparison between the computed contours and experimental results is made in figure 4. The dashed circles shown *do not correspond to the dimension of the nozzle*; they are drawn to accentuate the azimuthal dependence of the mean velocity. The data shown in figure 4(*a*, *b*) are replotted from figure 2(*a*, *b*). The data points shown in figure 4(*c*, *d*) are taken from the dissertation of Strange (1981), while the solid lines represent the solutions to (3.2). In this case, the jet was subjected to the standing waves generated by a combination of modes given by $m = \pm 2$ and the data were taken at $x/D = 2$ (figure 4*c*) and $x/D = 4$ (figure 4*d*). Since the waves are strongly amplified in this range of downstream distances, the contours shown in figure 4(*d*) correspond to a higher amplitude of excitation than the ones shown in figure 4*c*. Strange found that at $x/D = 12$, the azimuthal distribution of mean velocity regained its natural axisymmetric shape, probably because of the decay of the excited waves relative to the growing importance of random fluctuations.

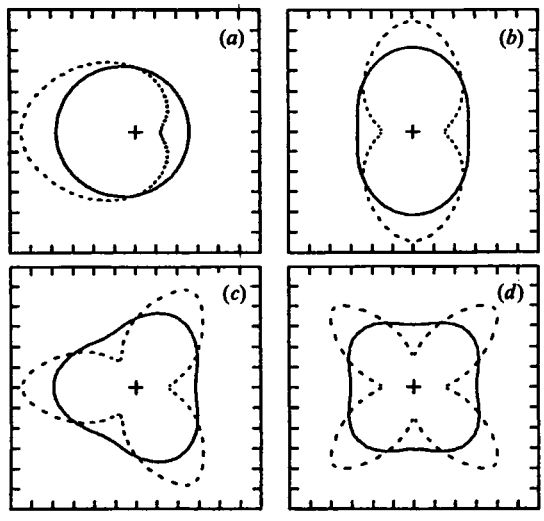

FIGURE 3. Theoretical iso-velocity contour plots, solutions of equation (3.2) with arbitrary scale and $U_{ac} = 0.5$: (*a*) $n = 1$; ——, $A = 0.2$; – – –, 0.45; (*b*) $n = 2$; ——, $A = 0.2$; – – –, 0.4; (*c*) $n = 3$; ——, $A = 0.15$; – – –, 0.4; (*d*) $n = 4$; ——, $A = 0.1$; – – –, 0.4.

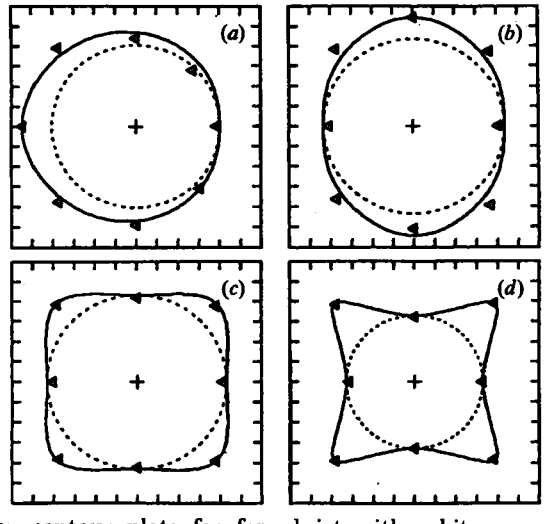

FIGURE 4. Iso-velocity contour plots for forced jet with arbitrary scale. (*a*) ◁, $m = 0+1$, $F_f = 204$ Hz, $x/D = 0.65$, $U_{ac} = 0.5$; ——, theoretical result (solution to equation (3.2)), $A = 0.45$; (*b*) ◁, $m = 0+2$, $F_f = 204$ Hz, $x/D = 0.65$, $U_{ac} = 0.5$; ——, theoretical result, $A = 0.4$; (*c*) ◁, $m = \pm 2$ (Strange 1981), $x/D = 2$, $U_{ac} = 0.2$; ——, theoretical result, $A = 0.11$; (*d*) ◁, $m = \pm 2$ (Strange 1981), $x/D = 4$, $U_{ac} = 0.2$; ——, theoretical result, $A = 0.18$. Dashed line represents an arbitrary circle for display purposes.

3.2. *The generation of resonant interactions*

Resonance conditions are demonstrated experimentally by subjecting the jet to one or two periodic oscillations whose frequency and azimuthal mode number can be carefully controlled. For externally excited flow, the resonance conditions given in (2.22) are reduced to

$$\beta_{in} = \beta_{11} + \beta_{12}; \quad \alpha_{in} = \alpha_{11} + \alpha_{12}; \quad m_{in} = m_{11} + m_{12}, \tag{3.3a}$$

$$\beta_{in} = \beta_{11} - \beta_{12}; \quad \alpha_{in} = \alpha_{11} - \alpha_{12}^*; \quad m_{in} = m_{11} - m_{12}. \tag{3.3b}$$

When one of the two disturbances is the subharmonic of the other one,

$$\beta_f \equiv \beta_{11} = 2\beta_{12} \equiv 2\beta_s, \tag{3.4}$$

where the subscript f represents the fundamental wave while s represents its subharmonic. The generation of a new subharmonic wave is possible according to (3.3*b*) provided

$$\beta_{in} = \beta_s, \tag{3.5a}$$

$$\alpha_{r,in} = \alpha_{r,f}(\beta_f) - \alpha_{r,s}(\beta_s), \tag{3.5b}$$

$$m_{in} = m_f - m_s, \tag{3.5c}$$

$$\alpha_{i,in} = \alpha_{i,f} + \alpha_{i,s}. \tag{3.5d}$$

The conditions represented in (3.5*a–c*) are associated with the periodic part of the wave, whereas the condition (3.5*d*) is associated with its amplitude. In the case of a slightly positive rate of growth, the amplitude of the wave can be redefined to include this growth rate, emphasizing the importance of the periodic conditions in comparison with the growth-rate condition.

When the excited waves are axisymmetric, the wave resulting from the resonant interaction is also axisymmetric [equation (3.5*c*)]. Equations (3.5*a*, *b*) can then be combined to yield

$$c_{pf} = c_{ps}, \tag{3.6}$$

where c_p is the phase velocity of the wave defined by $c_p = \beta/\alpha_r$. The condition inherent in (3.6) suggests that the fundamental wave will interact with its subharmonic, *provided both waves propagate at the same phase velocity*, allowing them sufficient time to interact and exchange energy.

The significance of (3.6) is demonstrated in the following two experiments. The phase velocity and the spatial growth rate, calculated by the linear stability theory based on the unperturbed mean velocity profile existing at $x/D = 0.75$, is shown in figures 5(*a*) and 5(*b*), respectively. The solid line represents the solution for the axisymmetric mode ($m = 0$), while the dashed line corresponds to the helical mode ($m = 1$). At a radial position at which the mean velocity was reduced to $\frac{5}{8}$ of its centreline value, power spectra of the streamwise component of velocity were measured. The spectral distribution in the absence of external excitation is shown in figure 6(*a*). The spectrum shown in figure 6(*b*) corresponds to the case in which the jet was subjected to an axisymmetric periodic disturbance at a frequency of 288 Hz. The emergence of the band of frequencies (figure 6*b*) centred around the subharmonic frequency (144 Hz), in addition to the sharp peak in the spectrum at the excitation frequency (288 Hz), was predicted with the resonance conditions since the phase speeds of both waves are almost identical (figure 5*a*). Conversely, strong excitation of the jet at an amplitude 100 times larger than the background but at a frequency of 144 Hz (figure 6*c*) did not result in any significant response at the subharmonic frequency of 72 Hz. The absence of a response is due to the difference in the phase velocities of the two waves (figure 5*a*), which did not fulfill the condition prescribed in (3.6).

The possibility that resonant conditions will generate an azimuthal mode not existing in the flow (equation (3.5*c*)) increases the range of probable nonlinear interactions. The results of an experiment exploring an intermodal resonant interaction is summarized in table 1. The jet was subjected to two periodic disturbances, a fundamental wave having a forcing frequency of $F_f = 288$ Hz and an azimuthal mode number $m_f = -1$, and a subharmonic wave with $F_s = 144$ Hz and $m_s = 0$.

The first line in table 1 shows the azimuthal amplitude distribution when the jet

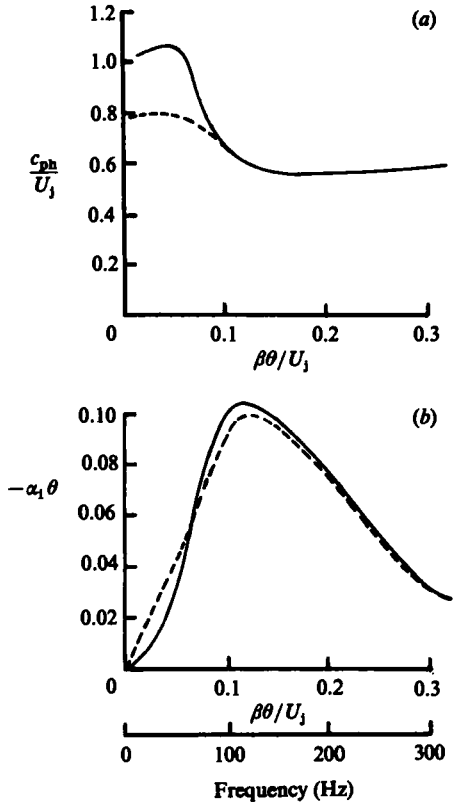

FIGURE 5. Eigenvalues calculated from parallel stability theory. $U_j = 810$ cm/s, $x/D = 0.75$, $\theta/D = 0.026$. Azimuthal mode: ——, $m = 0$; – – –, 1. (*a*) Phase velocity; (*b*) Spatial growth rate.

was subjected to a single disturbance. In both cases, where the jet was excited with a fundamental wave (288 Hz) or with a subharmonic wave (144 Hz), the largest component of the resulting azimuthal structure of the disturbance came from the excited mode number, i.e. $m = -1$ for $F_f = 288$ and $m = 0$ for $F_s = 144$ Hz. When the jet was subjected to both disturbances simultaneously, the azimuthal mode content of the amplitude distribution of the subharmonic wave was changed significantly, as shown in the second line of table 1.

The net gain of the subharmonic amplitude at $m = -1$ can be predicted theoretically from the resonance conditions (equation (3.5)). This is demonstrated in the third line of table 1, where the amplitude distribution corresponding to the single excitation is subtracted from that of the combined excitation, resulting in a net gain of the subharmonic disturbance in the $m_{in} = m_f - m_s = -1 - 0 = -1$ mode, which is equivalent to the excitation level at the $m = 0$ mode.

The modal decomposition of the waves demonstrated in table 1 enables one to distinguish which mechanism is responsible for the growth of the amplitude of a disturbance. The case illustrated in figure 6 was explained by the nonlinear interaction between the two waves whenever their phase velocities are matched. This case might have been partially explained by the linear stability theory; the subharmonic wave associated with figure 6(*b*) approximately at its maximum linear amplification rate (figure 5*b*), while the amplification rate of its subharmonic (figure 6*c*) is much lower. Such an explanation is not possible when one subdivides the results

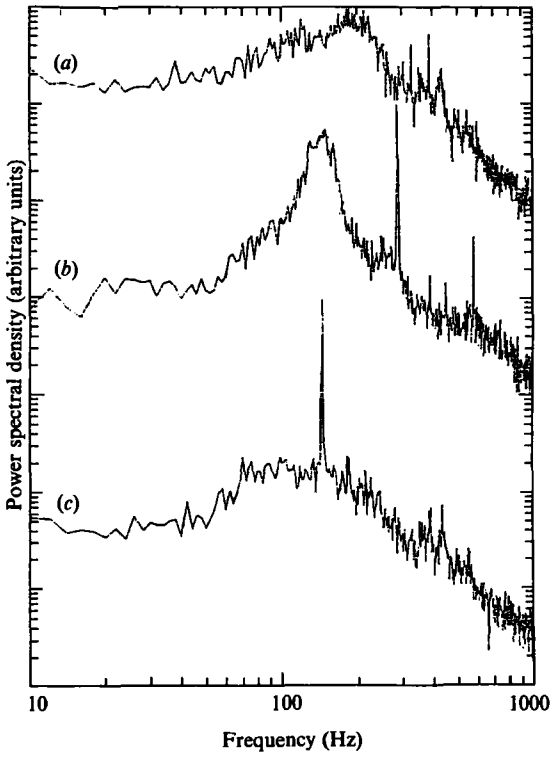

FIGURE 6. Subharmonic resonance: $x/D = 0.75$, $r = R_{0.625}$. (*a*) natural jet; (*b*) excitation at $F_f = 288$ Hz and $m = 0$; (*c*) excitation at $F_f = 144$ Hz and $m = 0$.

	Amplitude distribution (arbitrary scale)					
	$F_s = 144$ Hz; $m_s = 0$			$F_f = 288$ Hz; $m_f = -1$		
m	0	+1	−1	0	+1	−1
Single	*23.0*	1.9	1.4	1.17	10.0	*48.0*
Combined	24.2	8.8	22.3	4.1	10.7	47.5
Gain	1.2	8.0	*21.0*	3.0	0.7	−0.5

TABLE 1. Subharmonic resonance with $m_f = -1$ and $m_s = 0$

into azimuthal modes, as demonstrated in table 1. The linear stability theory cannot differentiate between $m = 1$ and $m = -1$ because the linear stability equation and the corresponding boundary conditions depend on the square of the azimuthal mode number m. Therefore, the fact that only the subharmonic wave at $m = -1$ gained most of its energy (table 1) *can only be explained by the nonlinear interaction between the two disturbances.*

Another example of subharmonic resonance is demonstrated in table 2. In this case, the resonance conditions given by (3.5) result in the generation of a new subharmonic wave running in a counterclockwise direction [$m_{in} = m_f - m_s = 0 - (-1) = +1$], whereas all of the input waves did not contain such a modal component (table 2, top line). The rapid generation of a subharmonic disturbance by a nonlinear resonance

	Amplitude distribution (arbitrary scale)					
	$F_s = 144$ Hz; $m_s = -1$			$F_f = 288$ Hz; $m_f = 0$		
m	0	+1	−1	0	+1	−1
Single	1.6	2.25	*43.9*	*40.8*	8.9	8.4
Combined	4.6	33.7	39.8	38.5	3.5	6.0
Gain	3.0	*31.5*	−4.0	−2.0	−5.4	−2.4

TABLE 2. Subharmonic resonance with $m_f = 0$ and $m_s = -1$

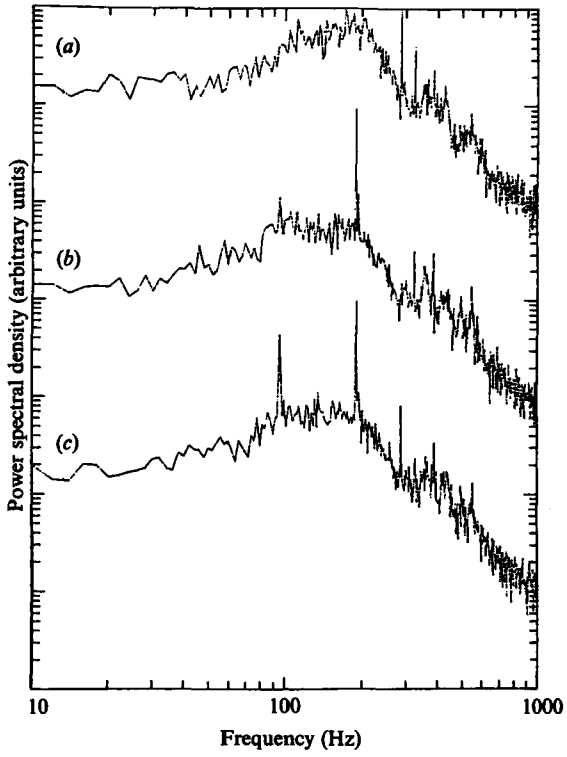

FIGURE 7. Resonance interaction between two axisymmetric wavetrains: $x/D = 0.75$, $r = R_{0.625}$. (*a*) Weak excitation at 288 Hz; (*b*) strong excitation at 192 Hz; (*c*) combined excitation.

may be synonymous with 'vortex pairing' for axisymmetric modes, which has been observed experimentally by Winant & Browand (1974).

Other kinds of nonlinear interactions are also possible (see Kelly 1967), as is demonstrated in figure 7. The spectral distribution of the axial velocity component for a jet subjected to an axisymmetric periodic disturbance at a frequency of 288 Hz is shown in figure 7(*a*). The level of excitation is so low that the spectral peak corresponding to the excitation frequency does not exceed the maximum peak in the spectrum occurring at 180 Hz, and the spectral distribution is almost identical with the one prevailing in an unexcited jet and given in figure 6(*a*). The spectral distribution corresponding to a strong excitation of an axisymmetric mode at a frequency of 192 Hz is shown in figure 7(*b*). The amplitude of the subharmonic

frequency, 96 Hz, did not significantly increase, because of the dispersion in phase velocities of both waves. However, when both excitations corresponding to figure 7(*a*, *b*) were combined, the resulting spectral distribution indicates a significant gain in the amplitude associated with the difference frequency of 96 Hz, fulfilling the resonance conditions outlined in (3.3*b*).

4. Concluding remarks

Instability modes in an axisymmetric jet are influenced by two lengthscales governing the mean flow on which these instabilities develop. The first is the local width of the shear layer, while the second is the diameter of the jet column limiting the number of evolving azimuthal modes. These two lengthscales govern the wavelengths and the most amplified instabilities and therefore also control the leading nonlinear interactions among them. Since in most laboratory jets the area ratio between the cross-section of the plenum chamber and the nozzle is large, only planar disturbances are emanating from the nozzle. The axisymmetric mode, therefore, plays a dominant role in the initial evolution of the jets so it is not surprising that large coherent structures in this configuration are still represented by vortex rings.

When the jet is excited by different azimuthal modes having the same frequency, the mean flow is distorted and the contours of mean velocity can no longer be represented by concentric circles. The actual shape of the velocity contours depends on the difference between the excited mode numbers and the local amplitude of the wave. Some of the predicted velocity distributions were experimentally observed (also see Strange 1981).

Whenever two disturbances attain a sufficiently high amplitude, the time-dependent nonlinear interaction between them is no longer negligible and a transfer of energy may occur from one wave to another, generating at times a third wave which was previously non-existent. The resonant conditions under which two disturbances can interact in an axisymmetric shear layer were predicted and demonstrated experimentally. The dominant interactions between two waves occur when one of the waves is a subharmonic of the other. Both waves must propagate downstream at the same speed (i.e. be non-dispersive) to allow sufficient time for the transfer of energy to take place. The large variety of nonlinear interactions possible in an axisymmetric jet mandate a careful analysis of many recessive linear modes which may be strongly amplified by the nonlinear process.

The authors would like to thank Dr. A. Newell for his assistance and enlightening discussions. The work was supported in part by the National Science Foundation under grant MEA 8210876 and by NASA grant NAG 3-460.

REFERENCES

Cohen, J. & Wygnanski, I. 1987. The evolution of instabilities in the axisymmetric jet. Part 1. The linear growth of disturbances near the nozzle. *J. Fluid Mech.* **176**, 191.

Kelly, R. E. 1967 On the stability of an inviscid shear layer which is periodic in space and time. *J. Fluid Mech.* **27**, 657.

Michalke, A. 1965 On spatially growing disturbances in an inviscid shear layer. *J. Fluid Mech.* **23**, 521.

MICHALKE, A. 1971 Instabilität eines kompressiblen runden Freistrahls unter Berücksichtigung des Einflusses der Strahlgrenzschichtdicke, *Z. Flugwiss.* **9**, 319.

PLASCHKO, P. 1979 Helical instabilities of slowly divergent jets. *J. Fluid Mech.* **92**, 209.

STRANGE, P. J. R. 1981 Spinning modes in orderly jet structure and jet noise. Ph.D. thesis, Dept. of Applied Mathematical Studies, University of Leeds, UK.

WINANT, C. D. & BROWAND, F. K. 1974 Vortex pairing, the mechanism of turbulent mixing layer growth at moderate Reynolds numbers. *J. Fluid Mech.* **63**, 237.